# Subcellular Distribution of α1G Subunit of T-type Calcium Channel in the Mouse Dorsal Lateral Geniculate Nucleus

Laxmi Kumar Parajuli,[1,2] Yugo Fukazawa,[1,2,3]* Masahiko Watanabe,[4] and Ryuichi Shigemoto[1,2,5]

[1]Division of Cerebral Structure, National Institute for Physiological Sciences, Okazaki, 444-8787, Japan
[2]Department of Physiological Sciences, Graduate University for Advanced Studies (SOKENDAI), Okazaki 444-8787, Japan
[3]CREST, Japan Science and Technology Agency, Tokyo 102-0075, Japan
[4]Department of Anatomy, Hokkaido University School of Medicine, Sapporo 060-8638, Japan
[5]SORST, Japan Science and Technology Agency, Kawaguchi 333-0012, Japan

## ABSTRACT

T-type calcium channels play a pivotal role in regulating neural membrane excitability in the nervous system. However, the precise subcellular distributions of T-type channel subunits and their implication for membrane excitability are not well understood. Here we investigated the subcellular distribution of the α1G subunit of the calcium channel which is expressed highly in the mouse dorsal lateral geniculate nucleus (dLGN). Light microscopic analysis demonstrated that dLGN exhibits intense immunoperoxidase reactivity for the α1G subunit. Electron microscopic observation showed that the labeling was present in both the relay cells and interneurons and was found in the somatodendritic, but not axonal, domains of these cells. Most of the immunogold particles for the α1G subunit were either associated with the plasma membrane or the intracellular membranes. Reconstruction analysis of serial electron microscopic images revealed that the intensity of the intracellular labeling exhibited a gradient such that the labeling density was higher in the proximal dendrite and progressively decreased towards the distal dendrite. In contrast, the plasma membrane-associated particles were distributed with a uniform density over the somatodendritic surface of dLGN cells. The labeling density in the relay cell plasma membrane was about 3-fold higher than that of the interneurons. These results provide ultrastructural evidence for cell-type-specific expression levels and for uniform expression density of the α1G subunit over the plasma membrane of dLGN cells. J. Comp. Neurol. 518:4362–4374, 2010.



**INDEXING TERMS:** Cav3.1; thalamus; electron microscopy; preembedding immunogold labeling; 3D reconstruction; dendrite

The opening of voltage-gated calcium channels (VGCC) leads to transient increases in intracellular $Ca^{2+}$. The location of calcium influx is strictly regulated to control the activation of calcium-dependent processes, such as neurotransmitter release, neuronal excitation, and regulation of gene expression. Biophysical and pharmacological studies have led to the identification of high-voltage-activated (HVA) calcium channels (L-, N-, P/Q-, and R-types) and a low-voltage-activated (LVA) T-type calcium channel (for reviews, see Jones, 1998; Catterall, 2000). Members of the HVA calcium channels require a larger membrane depolarization for their opening than the LVA T-type calcium channel. The latter is mostly inactivated at neuronal resting potential; thus, a brief hyperpolarization is required for the channel to deinactivate prior to activation (Jahnsen and Llinas, 1984; Perez-Reyes, 2003). Among the three different genes encoding T-type VGCC α1 subunits (Cav3.1/α1G, Cav3.2/α1H, and Cav3.3/α1I), the α1G subunit is highly expressed in the thalamus (Talley et al., 1999). It has been shown to play a prominent role in the generation of low-threshold spikes leading to



Additional supporting information may be found in the online version of this article.

Grant sponsors: SORST and CREST; Japan Science and Technology Agency (JST) (to R.S. and Y.F., respectively); Grant-in-Aid for Scientific Research on Priority Areas-Molecular Brain Sciences from the Ministry of Education, Culture, Sports, Science and Technology of Japan (MEXT); Grant numbers: 20019031 (to R.S.), 18022043 (to Y.F.).

*CORRESPONDENCE TO: Yugo Fukazawa, Division of Cerebral Structure, National Institute for Physiological Sciences, Okazaki 444-8787, Japan. E-mail: yugo@nips.ac.jp

Received December 7, 2009; Revised April 20, 2010; Accepted July 1, 2010
DOI 10.1002/cne.22461
Published online July 26, 2010 in Wiley Online Library (wileyonlinelibrary.com)

TABLE 1.
Primary Antibodies

| Target molecule | Code # in original lab or supplier | Host animal and clonality | Developer or supplier | Epitope amino acid residues | Optimal dilution |
|---|---|---|---|---|---|
| α1G subunit of T-type $Ca^{2+}$ channel | N/A | Guinea pig polyclonal affinity purified | Dr. Masahiko Watanabe | Amino acid residues 2269-2283 of the mouse Cav3.1 gene (CAI25956) | 1 μg/mL |
| Glutamic acid decarboxylase (GAD) | MAB351 | Mouse monoclonal (affinity purified IgG) | Chemicon | Purified rat brain GAD (Chang and Gottlieb, 1988) | 1 μg/mL |

N/A, not applicable.

thalamic burst firing and slow-wave sleep oscillations (Steriade et al., 1988; Huguenard, 1996; Kim et al., 2001; Lee et al., 2004; Song et al., 2004; Anderson et al., 2005).

Neuronal excitability is thought to be dependent on the precise spatial distribution of voltage-gated ion channels. In the thalamus, although previous studies have suggested postsynaptic expression (dendrites and soma) of the α1G channel subunit, their relative distribution along the somatodendritic axis of the thalamic neurons has not yet been fully elucidated and is a matter of debate. An earlier electrophysiological and computational modeling study suggested an enrichment of this subunit in the distal part of the dendrite (Destexhe et al., 1998), whereas others have suggested its predominant somatic and proximal dendritic localization (Munsch et al., 1997; Zhou et al., 1997; Williams and Stuart, 2000; Zhuravleva et al., 2001; Rhodes and Llinas, 2005). In a recent computational modeling study, it was suggested that the appropriate thalamic oscillation can be achieved even if the T-type calcium channels are distributed uniformly throughout the somatodendritic arbor (Zomorrodi et al., 2008). Although informative, the data obtained from these previous studies remain largely speculative due to the lack of a selective T-type calcium channel blocker and unequivocal criteria to define the T-type current. Furthermore, these studies are technically constrained due to the seemingly challenging limitation of resolving the calcium signals from the fine-caliber distal dendrites. Therefore, a precise and quantitative subcellular localization of this channel has been the subject of considerable interest.

Immunoelectron microscopy is an indispensable method for studying the ultrastructural localization of channel molecules. However, to date our potential understanding of the α1G distribution has been hampered by the lack of specific antibodies against this subunit applicable for immunoelectron microscopy. In this study, to reveal the relative distribution of the α1G subunit in the somatodendritic axis of the dorsal lateral geniculate nucleus (dLGN) neurons, we used a newly developed antibody specific for the mouse α1G subunit and employed high-resolution immunoelectron microscopy. Our results demonstrate a uniform distribution of the α1G subunit over the somatodendritic plasma membrane of the dLGN neurons.

## MATERIALS AND METHODS

### Animals

Ten 8-week-old male wildtype (WT) mice (C57BL/6NCr Slc) and four 8-week-old α1G-deficient mice (Kim et al., 2001) were used for this study. The animals were raised in a normal light/dark cycle with free access to food and water. Efforts were made to minimize the number of animals and pain and suffering of the animals used. All experimental procedures performed on the animals were carried out in accordance with the guidelines of animal care and use committee of the National Institute for Physiological Sciences (Okazaki, Japan) and approved by the committee.

### Fixation

For light microscopic observation, mice were deeply anesthetized with sodium pentobarbital (intraperitoneal [i.p.], 50 mg/kg body weight) and perfused with 25 mM phosphate-buffered saline (PBS) for 1 minute followed by a fixative containing 4% paraformaldehyde and 15% saturated picric acid in 0.1 M phosphate buffer (PB, pH 7.4). For electron microscopic observation, anesthetized mice were fixed with the same fixative solution containing 0.1% glutaraldehyde (Polysciences, Warrington, PA). After fixation the brain was cut coronally on a slicer (Leica, VT-1000, Austria) at a thickness of 50 μm for both light and electron microscopic analysis. The sections were washed twice in PB and then further processed for immunolabeling.

### Antibody characterization

Primary antibodies used in this study are listed in Table 1. A guinea pig polyclonal antibody for the α1G subunit of the T-type calcium channel was raised against the C-terminal sequence of mouse Cav3.1. The specificity of this anti-α1G antibody has been previously tested and confirmed by immunohistochemistry in light microscopy (Hildebrand et al., 2009). The previous study demonstrated that the intense immunofluorescent signal observed in

the cerebellum and thalamus of the WT mouse was absent in the brain sections from α1G knockout (KO) mouse. In the present study we further confirmed the specificity of the antibody. At both the light microscopic and electron microscopic levels, the strong labeling observed in the thalamus of the WT mouse was abolished in the α1G KO mice (Fig. 1; Supporting Figs. 1, 2), thereby providing evidence for the specificity of our immunolabeling. A mouse monoclonal antibody for glutamic acid decarboxylase (GAD; Chemicon, Temecula, CA; MAB351) used in this study has been shown to recognize the lower molecular weight isoform (65 kDa) of the two GAD isoforms identified in the brain (Chang and Gottlieb, 1988).

## Immunohistochemistry for light microscopy

Fixation, labeling conditions, and antibody concentration were rigorously optimized during our initial pilot experiments. Sections were blocked with 10% normal goat serum (NGS; Vector Laboratories, Burlingame, CA) and 0.1% Triton X-100 in PBS for 1 hour and then incubated overnight at 4°C with the primary antibody against α1G (1 μg/mL) in PBS containing 2% NGS and 0.05% Triton X-100. After several washes in PBS, sections were incubated with a biotinylated goat anti-guinea pig IgG antibody (1:200; Vector Laboratories) diluted in PBS containing 2% NGS and 0.05% Triton X-100 at room temperature for 1 hour. The sections were washed with PBS and reacted with avidin-biotin peroxidase complex (1:100 ABC-Elite; Vector Laboratories) diluted in PBS containing 0.1% Triton X-100 for 1 hour at room temperature. After washing three times in PBS the sections were washed once in 50 mM Tris-HCl buffer (pH 7.6) and then incubated at room temperature in the buffer supplemented with 0.025% 3,3′-diamino benzedine tetrahydrochloride (DAB; Dojindo Lab., Kumamoto, Japan) and 0.003% hydrogen peroxide. Upon reaching the appropriate signal intensity, the DAB reaction was terminated by incubation in PB. Sections were mounted on glass slides, dehydrated in graded alcohol, and covered with coverslips. Digital images were obtained with a BX50 microscope equipped with a DP70 digital camera (Olympus, Tokyo, Japan). The images for WT and the KO sections were taken under the same conditions (e.g., light intensity, exposure time) and adjusted for brightness and contrast identically and uniformly in Photoshop CS2 (Adobe, San Jose, CA) for preparation of figures.

## Electron microscopic immunoperoxidase labeling

Sections were cryoprotected in a solution containing 25% sucrose and 10% glycerol in 20 mM PB and freeze-thawed with liquid nitrogen. After several washes in 50 mM Tris-HCl buffered saline (TBS), the sections were incubated with the blocking solution containing 20% NGS in TBS for 1 hour and then processed similarly as described for light microscopic immunohistochemistry except that Triton X-100 was omitted in all the steps. After the development of immunoperoxidase reaction, sections were fixed with 1% $OsO_4$ for 40 minutes, stained with 1% uranyl acetate for 35 minutes, dehydrated, and flat-embedded in Durcupan resin (ACM Fluka, Sigma-Aldrich, Gillingham, Dorset, UK). Ultrathin sections of 70 nm thickness were prepared using an ultramicrotome (Ultracut T; Leica), poststained briefly with lead citrate, and observed under a transmission electron microscope (EM208S; Philips, Eindhoven, The Netherlands). Digital images were obtained using a MegaView III CCD camera (Olympus-SIS, Germany) and processed with iTEM software (Olympus-SIS) for image analysis. For preparation of figures, brightness and contrast of images were adjusted uniformly over the entire image with Photoshop CS2.

Three-dimensional reconstructions of neuronal profiles were carried out with serial ultrathin sections using a freeware, Reconstruct, provided through the Synapse Web (Fiala, 2005).

## Electron microscopic immunogold labeling

Sections were freeze-thawed as described above. After several washes in TBS, the sections were blocked with 5% acetylated bovine serum albumin (BSA-C; Aurion, Wageningen, The Netherlands) and 5% NGS in PBS for 1 hour. The sections were then washed twice with PBS containing 0.2% BSA-C (PBS/BSA-C) and incubated overnight at 4°C with the α1G antibody diluted at 1 μg/mL in PBS/BSA-C. After washing with PBS/BSA-C, sections were incubated overnight at 4°C with 0.8-nm gold conjugated goat anti-guinea pig secondary antibody (1:100; Aurion) diluted in PBS/BSA-C. After several washes with PBS-BSA/C, the sections were further washed four times for 10 minutes each with enhancement conditioning solution (ECS; Aurion). The sections were then silver-intensified with the R-Gent SE-EM intensification kit (Aurion). After washing, the sections were fixed with 1% $OsO_4$, stained with uranyl acetate, dehydrated, and flat-embedded in Durcupan resin.

Double immunolabeling was performed using the guinea pig polyclonal antibody against α1G and the mouse monoclonal antibody against GAD. Sections were incubated in a mixture of the anti-α1G (1 μg/mL) and anti-GAD (1 μg/mL) antibodies. After overnight incubation with biotinylated anti-mouse (1:100; Vector Laboratories) and gold-conjugated goat anti-guinea pig secondary antibodies (1:100; Aurion), we proceeded first with the immunogold method for α1G up to the silver

enhancement and then with ABC method followed by a peroxidase reaction for GAD.

## Quantification of immunoparticles

Among various nuclei of the thalamus, this study particularly focused on the dLGN because its neural circuitry has been well characterized and the electrophysiological properties of neuronal cells in this nucleus has been extensively studied. In addition, the dLGN in rodents is the only thalamic nucleus containing both principal neurons and local circuit interneurons (Ohara et al., 1983; Paxinos, 1995; Arcelli et al., 1997), thus conferring the unique possibility of comparing the α1G expressions between these two different neuronal cell types.

The subcellular distribution of α1G was analyzed from two WT mice for single labeling and one WT mouse for double labeling. In order to sample the profiles within the optimal penetration depth of the antibody, electron micrographs were obtained within 1–3 μm from the resin–tissue interface. To ascertain that a specific dendrite is immunolabeled, we examined the dendrites in 20–30 serial ultrathin sections collected on the same grid for quantification purposes.

In the single-labeling experiment, the relay cells were distinguished from the interneurons based on their morphological criteria. Any dendritic profiles containing flattened and pleomorphic synaptic vesicles were identified as interneuron processes. Somatic profiles were identified as interneurons if they have a small somatic diameter with nuclear infoldings (Jones, 2007). When encountered, such processes were omitted from the quantification study performed from the single-labeling experiment, which focused only on the relay cell processes. However, it should be noted that our electron microscopic immunolabeling study makes use of a mild tissue fixation condition which hinders the optimal ultrastructural preservation. Thus, to investigate labeling in interneurons, GAD immunoreactivity was used as a marker for reliable distinction of interneurons from the relay cells in another separate set of experiments.

The retinogeniculate axon terminal was distinguished from the corticogeniculate axon terminal based on their morphological features. Large terminals containing round synaptic vesicles and pale mitochondria were identified as retinogeniculate terminals, whereas small terminals containing round synaptic vesicles and dark mitochondria were identified as corticogeniculate terminals (Lieberman and Webster, 1974).

Twenty-eight different dendritic segments and three different somatic segments were reconstructed from 20–25 serial ultrathin sections. The dendritic diameter of individual reconstructed profiles was measured as the widest transect of the narrowest dimension of the ovoid profile of the dendrite (Hanson and Smith, 2002). A dendritic diameter is an indirect measure of the distance from the soma, since the minor diameter of a dendrite progressively decreases with increasing distance from the soma. Linear density of the gold particles in the plasma membrane was obtained by dividing the total number of plasma membrane-bound immunogold particles (see text for the criteria) by plasma membrane length of individual reconstructed dendrites. Dendritic surface area was calculated by multiplying the total plasma membrane length of each reconstructed dendrite by the section thickness (70 nm). The total number of plasma membrane-bound gold particles found in a reconstructed dendrite was divided by the dendritic surface area to obtain the labeling density of plasma membrane-bound particles in individual profiles. For calculating the density of internal membrane-bound particles, the total number of intracellular particles found in a profile was divided by the dendritic cross-sectional area.

Synaptic, perisynaptic, and extrasynaptic areas were defined according to the method described by Barthó et al. (2004). Briefly, the synaptic area was calculated from synaptic lengths in a series of EM images and the section thickness (70 nm) as shown in the formula below.

$$A_{syn} = [(l_{first} + l_{second}) + (l_{second} + l_{third}) + \cdots + (l_{last-1} + l_{last})] \times 0.07/2$$

where $l_{first}$, $l_{second}$, $l_{third}$, $\ldots l_{last}$ refer to the synaptic length of the first, second, third, ... last section of the series containing the given synapse. Perisynaptic plasma membrane area, defined as an annulus surrounding a synapse by 200 nm in this study, was determined by an approximation of the area occupied by two rectangles on the top and bottom of the synapse, two parallelograms on the sides of the synapse, and four quarters of a cycle connecting the rectangles and the parallelograms. It can be formulated as:

$$A_{perisyn} = (l_{first} \times 0.2) + (l_{last} \times 0.2) + [0.2 \times 0.07 \times (n-1) \times 2] + (0.2^2 \times 3.14)$$

where n refers to the number of sections containing that synapse. Extrasynaptic areas were obtained after subtracting the synaptic and perisynaptic areas from the total surface area of the reconstructed dendrites. In order to compare labeling densities for α1G between perisynaptic and extrasynaptic areas, only dendrites in which synapses located within at least three sections (≈210 nm) inside from the top and bottom edge of the reconstructed dendrite were used. Out of 28 reconstructed dendrites, this analysis criterion was fulfilled by six dendrites. A total of nine synapses were found in

these six dendrites. Membrane-bound particles for α1G were divided into two groups as perisynaptic particles and extrasynaptic particles, and the labeling densities within the two membrane domains in individual profiles were calculated.

### Statistical analysis

Statistical analysis was performed using SPSS (Chicago, IL). Shapiro-Wilk's W-test was applied for checking the normality of the datasets. The statistical significance between groups was analyzed by the two-tailed unpaired Student's *t*-test and Mann–Whitney *U*-test for parametric and nonparametric analysis, respectively. One-way analysis of variance (ANOVA) was used for statistical comparison among multiple groups. Correlation analysis was performed using Spearman's rank order test. Statistical significance was defined as $P < 0.05$. The data in the text are expressed as mean ± SEM.

## RESULTS

### Distribution of immunoreactivity for α1G in the thalamus

At the light microscopic level, immunolabeling for α1G revealed a specific pattern of α1G distribution in the thalamic nuclei. A majority of the thalamic nuclei exhibited a moderate to strong labeling for α1G (Fig. 1 and Supporting Fig. 1). A strong immunoreactivity was observed in the midline thalamic nuclei (e.g., paraventricular thalamic nucleus and reuniens nucleus), anterior thalamic nuclei (e.g., laterodorsal thalamic nucleus), medial thalamic nuclei (e.g., mediodorsal thalamic nucleus), and ventral motor nuclei (e.g., ventral lateral, ventral medial). Intralaminar nuclei such as the parafasicular nucleus had a moderate level of α1G immunoreactivity. In the epithalamus, the lateral habenular nucleus showed a strong immunoreactivity, whereas the immunosignal in the medial habenular nucleus was weak. In the geniculate complex, dLGN and the magnocellular part of ventral LGN showed strong reactivity compared to the very weak immunoreactivity observed in the parvocellular part of ventral LGN. The ventrobasal nucleus, one of the major thalamic relay nuclei, also showed a strong immunoreactivity for α1G. The dLGN, which is the visual first-order relay nucleus, had a stronger immunoreactivity than its corresponding higher-order counterpart nuclei, that is, the lateral posterior nucleus. In contrast to the dLGN, the labeling in the thalamic reticular nucleus (TRN), which contains no relay cells, was below the detection limit (Supporting Fig. 1). No immunoreactivity for α1G was detected in the white matter. The α1G labeling observed in the WT mice was completely abolished in the KO animals (Fig. 1, Supporting Figs. 1, 2).

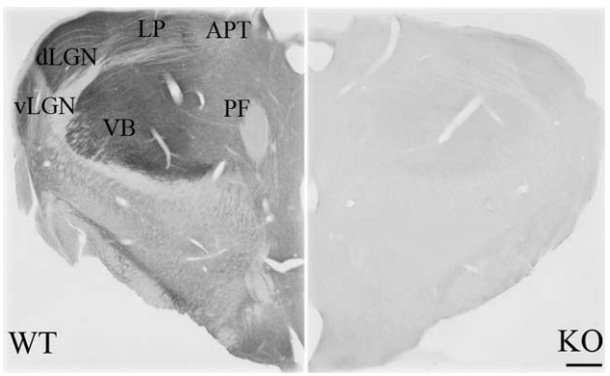


**Figure 1.** α1G immunoreactivity in the mouse thalamus. Light microscopic immunoperoxidase staining for α1G in the coronal brain slice showed intense immunoreactivity in several thalamic nuclei in the WT mouse but not in the α1G KO mouse. APT, anterior pretectal nucleus; dLGN, dorsal lateral geniculate nucleus; LP, lateral posterior thalamic nucleus; PF, parafascicular nucleus; VB, Ventrobasal nucleus; vLGN, ventral lateral geniculate nucleus. Scale bar = 250 μm.

### Electron microscopic observation of α1G immunoreactivity in the dLGN

The immunoperoxidase reaction was performed to determine the distribution of α1G immunoreactivity at the subcellular level. The peroxidase reaction endproduct was observed exclusively in dendrites and somata but not in axons and presynaptic terminals (Fig. 2A). Qualitatively, a large number of dendrites were positive for α1G. Peroxidase labeling revealed that the dendrites postsynaptic to putative retinal as well as cortical terminals were both immunopositive.

Next, to reveal the precise location of the channels at a greater spatial resolution, immunogold labeling was performed. Immunogold particles for α1G were observed in small- and large-caliber dendrites as well as in the somata in close correspondence with the peroxidase labeling (Fig. 2B,C). The gold particles were localized intracellularly as well as in close proximity to the plasma membrane. Virtually no immunoparticles for α1G were observed in the slices obtained from the KO animal (Supporting Fig. 2).

### Distribution of α1G immunogold particles in relation to membrane structures

To analyze the location of immunogold particles relative to the nearest membrane structures, the distance from the center of the individual gold particles to the middle of the nearest membrane structures were measured in one WT specimen. The measured distance for each gold particle was subjected to histogram analysis with a bin width of 5 nm and plotted against the frequency of profiles (Fig. 3). Although the distance distribution of the

gold particles did not follow a Gaussian distribution ($P < 0.001$, n = 179), the data plot revealed a single peak at 10–15 nm (mean = 16.6 ± 0.82 nm, median = 14.6 nm), thereby suggesting that those immunoparticles are bound to molecules expressed in the membranes.

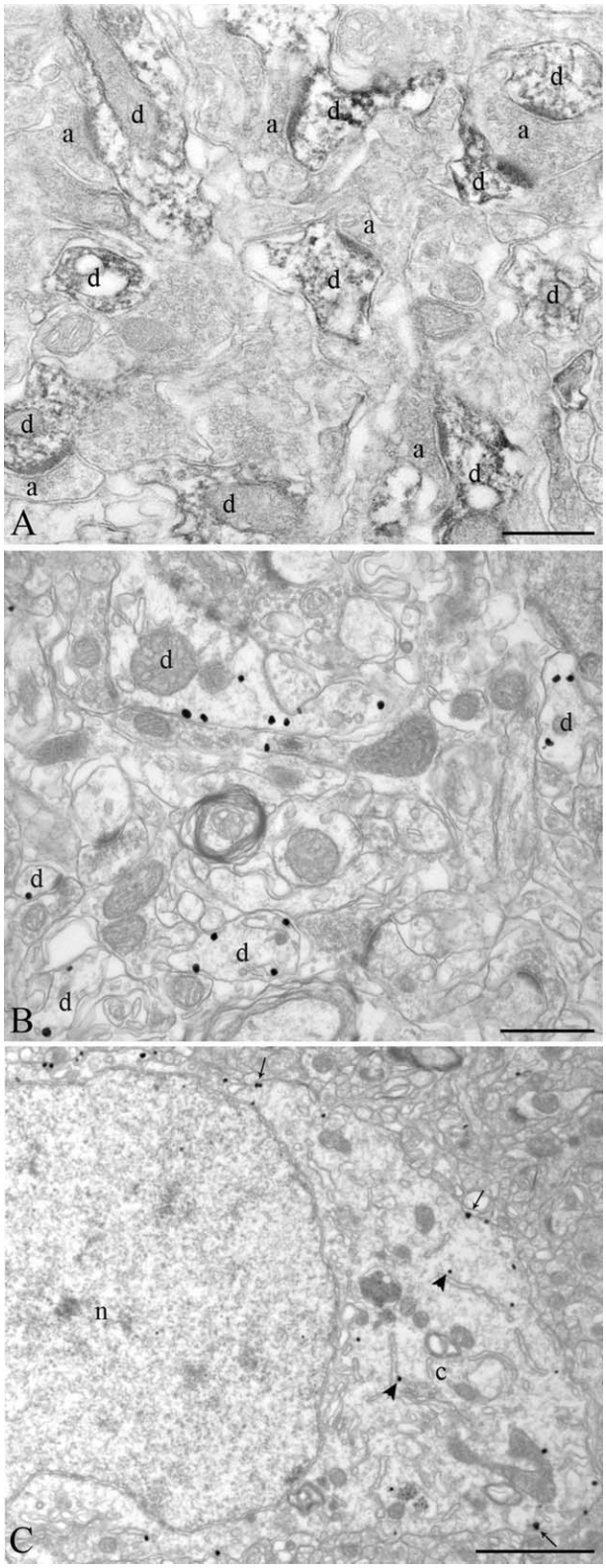


## Relative proportion of the plasma membrane- and intracellular membrane-bound α1G immunogold particles in the dendritic domains of the dLGN relay neurons

To quantify the proportion of α1G present in the plasma versus intracellular membranes, we recategorized all the immunoparticles either as plasma membrane- or internal membrane-bound. Based on the particle distribution histogram presented in Figure 3, about 95% of the immunoparticles were located within 42 nm (mean + 2 SD) from the membrane structures. Thus, particles located within 42 nm from the plasma membrane towards the cell interior were categorized as plasma membrane-bound particles and the rest of them as intracellular membrane-bound particles (Fig. 4). From a total of 1,284 immunogold particles analyzed, 118 particles were observed in the small-caliber (<0.5 μm) distal dendrites (n = 9), of which 98 (83%) were plasma membrane-bound and 20 (17%) were internal membrane-bound. Of 143 particles observed in the medium-caliber (0.5–1.0 μm) dendrites (n = 7), 94 (65.7%) were plasma membrane-bound and 49 (34.3%) were internal membrane-bound. In the large-caliber (>1.0 μm) proximal dendrites (n = 12), 1,023 particles were observed, of which 400 (39.1%) were plasma membrane-bound and 623 (60.9%) were internal membrane-bound. In total, 592 (46.1%) particles were found to be associated with the plasma membrane and the remaining 692 (53.9%) particles were associated with the internal membrane.

## Densities of α1G immunogold particles over somatodendritic compartments of dLGN relay neurons

In recent years, a number of studies have shown that certain ion channel molecules can be selectively targeted to specific membrane compartments. In dLGN, previous electrophysiological studies have suggested an uneven distribution of T-type calcium channels between the

**Figure 2.** Immunoreactivity for α1G was found exclusively in postsynaptic elements in the dLGN. Immunoperoxidase staining and immunogold labeling for α1G in the mouse dLGN were investigated by electron microscopy. The peroxidase reaction endproduct was observed exclusively in the dendrites but not in the presynaptic compartments (**A**). Electron micrographs showing the localization of the immunogold particles in the dendritic regions (**B**) and soma (**C**) demonstrate that the immunoparticles were found not only in close proximity to the plasma membrane (arrows) but also deep in the cytoplasm (arrowheads). a, presynaptic axons; c, cytoplasm; d, dendrite; n, nucleus. Scale bars = 500 nm in A; 800 nm in B; 1.5 μm in C.

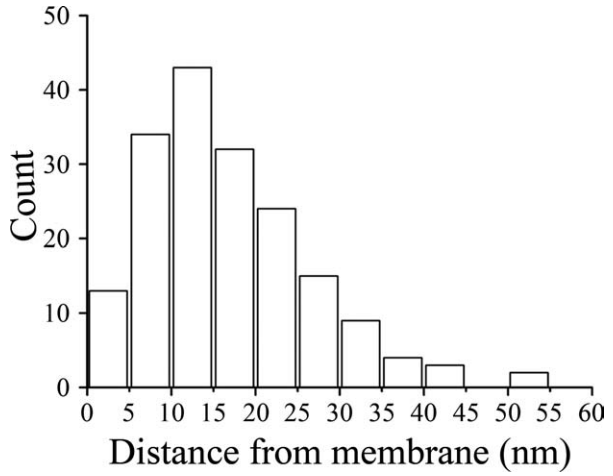


**Figure 3.** Immunogold particles for α1G were associated with membrane structures. Location of immunoparticles for α1G was measured in relation to the nearest membrane structures. The values were allocated to 5-nm-wide bins and expressed as count. The frequency distribution of the particles (n = 179) plotted against their distance from the nearest membrane structure showed a single peak lying at 10–15 nm (mean = 16.6 nm and median = 14.6 nm). Approximately 95% of the immunoparticles were within 42 nm from the membranes, suggesting that the particles were bound to epitopes present in the cellular membranes.

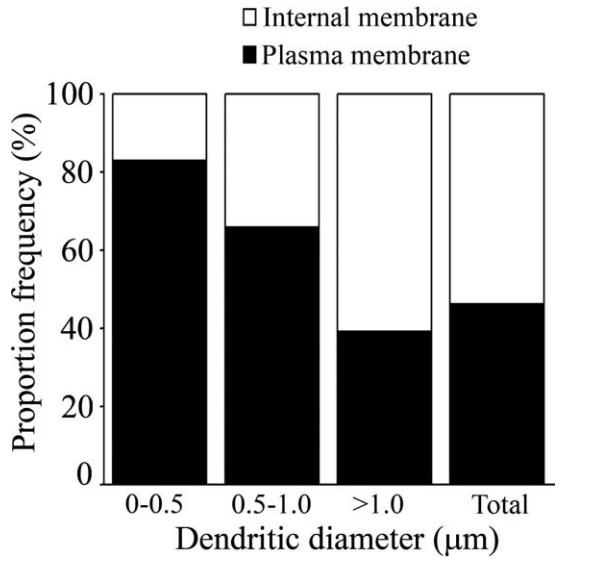


**Figure 4.** Proportion of plasma membrane-bound immunoparticles for α1G. Bar graphs showing relative proportions of the plasma membrane-bound particles which were estimated in 28 reconstructed dendrites and analyzed in relation to the diameter of individual profiles. A total of 1,284 immunoparticles were analyzed. Note that the large-caliber dendrites showed a higher proportion of internal labeling (see text). In total, 46.1% of the particles were plasma membrane-bound, whereas the rest of the particles (53.9%) were located intracellularly.

somata and the dendrites (Munsch et al., 1997; Zhou et al., 1997; Destexhe et al., 1998; Williams and Stuart, 2000; Zhuravleva et al., 2001; Rhodes et al., 2005). We therefore aimed to determine if indeed α1G shows such compartmental distribution in the somatodendritic domains of dLGN cells. In serial sections, the immunogold particles for α1G were observed both in the small- and large-caliber dendrites (Fig. 5A–H). No correlation between the dendritic diameter and the immunogold linear density was detected (Fig. 6A, $r = -0.209$, $P = 0.286$, n = 28). Similarly, there was no significant difference in the immunogold density between the somatic (0.194 ± 0.004 particle/μm, n = 3) and dendritic (0.182 ± 0.012 particle/μm, n = 28) compartments ($P = 0.640$, Mann–Whitney *U*-test). Mean linear density values correspond to 2.77 particle/$\mu m^2$ (2.71–2.88) and 2.60 particle/$\mu m^2$ (range 1.01–4.71) in the somatic and dendritic compartments, respectively. It is also important to mention that there was a high variability in the labeling density even among the dendrites of similar dendritic diameters (Fig. 6A). Similar proximodistal distribution and labeling patterns were obtained from another WT animal in which 30 dendritic segments and six somatic segments were reconstructed from 28–30 serial ultrathin sections collected on a single grid (data not shown).

Since a large fraction of immunoparticles were found to be associated with the intracellular membranes, we quantified and compared the intracellular labeling density with that of the plasma membrane labeling. When the proportion of intracellular membrane-bound immunogold particles was examined in relation to the dendritic diameter, a weak positive correlation was observed (for related information, see Fig. 4, $r = 0.909$, $P < 0.001$, n = 28). Moreover, the density of intracellular membrane-bound particles also increased with dendritic diameter (Fig. 6B, $r = 0.559$, $P = 0.002$, n = 28). This suggests that the higher intracellular labeling in the proximal part is not merely due to the larger volume of the profile but due to the specific localization of these molecules to the intracellular membranes.

## No accumulation of immunogold for α1G nearby synaptic junctions

At the electron microscopic level, it has been shown that the α1A and α1G subunits of calcium channels were localized mainly in the dendritic spines in the cerebellum, suggesting the role of these channels in synaptic events (Kulik et al., 2004; Hildebrand et al., 2009). In the present study, even though in some cases the gold particles for α1G were observed near the synapse, no clear preference of the gold particles for the synaptic, perisynaptic, or extrasynaptic sites could be established in the serially reconstructed dendrites (Fig. 5I–L). Rather, the immunoparticles

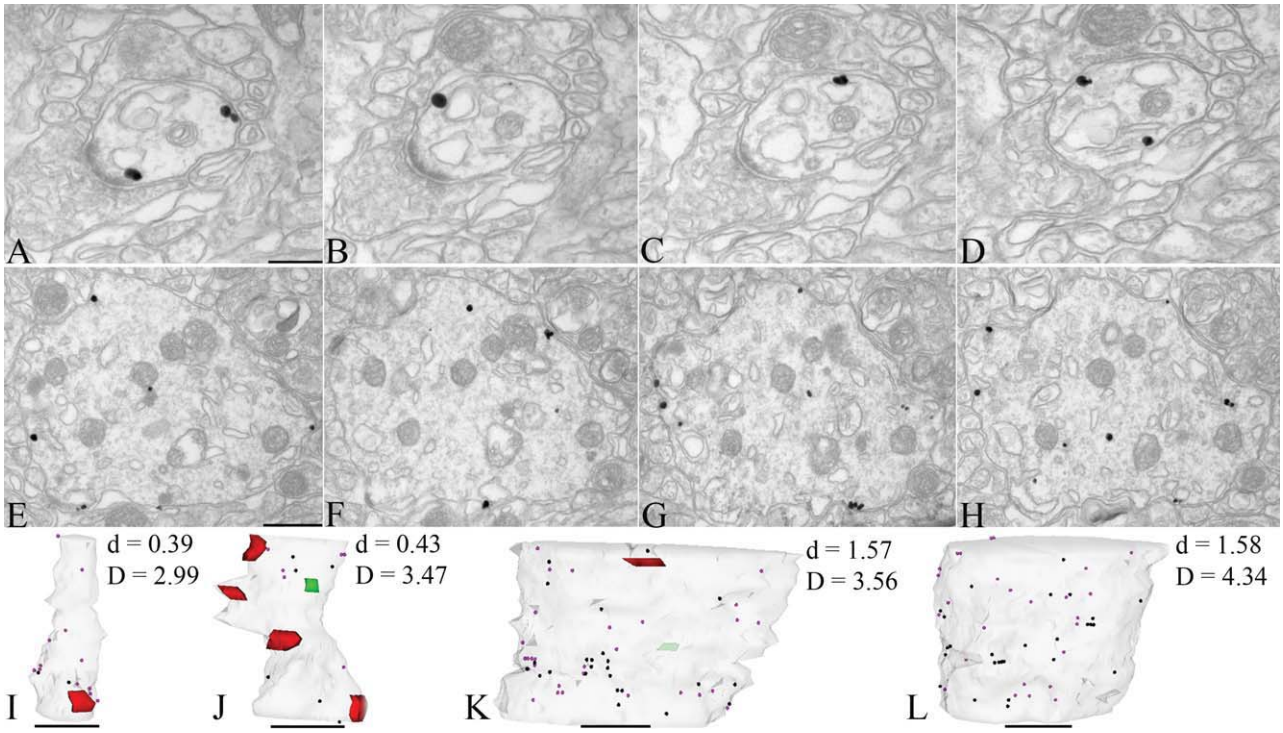


**Figure 5.** Three-dimensional reconstruction of labeled dendrites. Consecutive serial pictures show α1G immunogold labeling in the small-caliber dendrite (**A–D**) and in the large-caliber dendrite (**E–H**). Four dendrites with membrane-bound particles reconstructed from 28 serial electron micrographs are shown (**I–L**). Asymmetrical synapses (excitatory) are represented by red and symmetrical synapses (inhibitory) are represented by green. Particles in black represent particles facing towards the observer and particles in pink represent those on the opposite face of the dendritic arbor. The faint green synapse in K is located on the opposite face of the arbor. Note that the immunoparticles (total 132 particles) were distributed randomly over the dendritic plasma membrane without any noticeable preference to the synaptic sites. d, dendritic diameter; D, labeling density (particle/$\mu m^2$). Scale bars = 200 nm in A–D; 500 nm in E–H,I–L.

were found to be diffusely scattered all over the dendritic plasma membranes.

This qualitative observation was further supported by the results obtained from the quantitative analysis of the immunogold density in relation to the perisynaptic (an annulus surrounding a synapse by 200 nm) and extrasynaptic areas. The average immunogold densities were 3.34 ± 0.96 (range 0.00–7.25, n = 9) particles/$\mu m^2$ and 3.13 ± 0.26 (range 1.76–3.89, n = 6) particles/$\mu m^2$ in the perisynaptic and extrasynaptic areas, respectively, and were not significantly different ($P = 0.841$, unpaired Student's *t*-test).

## α1G labeling in interneurons

Despite the wealth of data about the expression of T-type calcium channels in principal neurons, little is known about their expression in interneurons. With this incentive, double labeling for GAD and α1G was performed to analyze α1G distribution in the GABAergic interneuron. Figure 7 shows two consecutive serial sections with a GAD-positive interneuron dendrite (i) and a relay cell dendrite (r) located adjacent to each other. The relay cell dendrite was well labeled in comparison to the interneuron dendrite. Serial reconstruction analysis (10–15 sections) revealed a linear density of 0.063 ± 0.015 particle/μm in the dendritic (n = 19) and 0.026 ± 0.022 particle/μm in the somatic compartments (n = 3) of the interneuron, with no significant difference ($P = 0.356$, Mann–Whitney *U*-test). GAD negative dendritic profiles representing an obvious relay cell population had a linear density of 0.206 ± 0.021 in the dendritic (n = 22) and 0.244 ± 0.037 particle/μm in the somatic (n = 3) compartments. These density values for the relay cell were not significantly different from those obtained from the single-labeling experiment. The quantitative analysis revealed 3.3-fold higher labeling density in the plasma membrane of the relay cell dendrite when compared to the interneuron dendrite ($P < 0.001$, Mann–Whitney *U*-test). Moreover, this difference was as high as 9.4-fold in the case of labeling densities between the somatic compartments of these two cell populations ($P < 0.001$, Mann–Whitney *U*-test). This suggests that despite the presence of α1G channels in interneurons, they were expressed at much lower levels when compared to those in the relay cells.

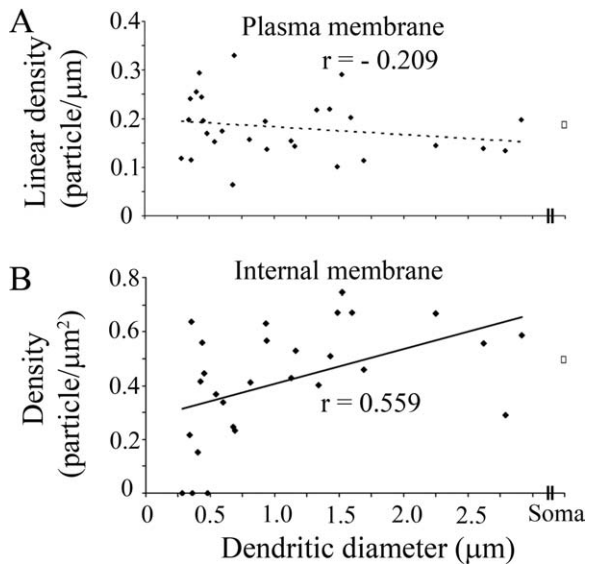


**Figure 6.** α1G immunoparticles were observed uniformly over the somatodendritic domains of the plasma membrane. **A**: Density of immunogold particles for α1G associated with the plasma membrane was measured in serial section electron micrographs (n = 28 for dendrites; n = 3 for somata) and plotted against the diameter of individual profiles. The filled dots represent the labeling densities of individual relay cell dendrites, and the open rectangle represents the average labeling density in the relay cell soma. No correlation was observed between the dendritic diameter and the immunogold density ($r = -0.209$, $P = 0.286$). Note that there was a large variability in the immunogold density even among the dendrites with similar dendritic diameters, and the variability was more pronounced in the small-caliber dendrites compared to the larger-caliber proximal dendrites. **B**: Number of internal membrane-bound immunogold particles for α1G was divided by the cross-sectional area of individual profiles and plotted against the diameter of the profile. The intracellular labeling density for α1G was highest at the proximal dendrites and decreased gradually towards the small-caliber dendrites. A positive correlation was found between the density of the α1G particles and the dendritic diameter ($r = 0.559$, $P = 0.002$, n = 28 for dendrites; n = 3 for somata).

We also examined whether the interneurons showed any preference in α1G expression in relation to the dendritic diameter. The average linear densities of immunogold particles associated with interneuron dendrites of different diameters were 0.054 ± 0.048 particle/μm, 0.064 ± 0.034 particle/μm, and 0.086 ± 0.034 particle/μm in the small-caliber (<0.5 μm), medium-caliber (0.5–1.0 μm), and large-caliber (>1.0 μm) dendrites, respectively (Fig. 8). There were no significant differences in the relative abundance of the labeling among these compartments (one-way ANOVA, $F_{2,16} = 0.260$, $P = 0.775$). Again, the plasma membrane of the relay cells showed a uniform labeling density among different dendritic compartments in this double-labeling experiment (one-way ANOVA, $F_{2,19} = 0.016$, $P = 0.984$). These observations further corroborate the uniform proximodistal distribution of α1G channels in the plasma membrane of dLGN cells.

## DISCUSSION

The spontaneous rhythmic activities of thalamic relay cells crucially depend on the T-type calcium channel and most importantly on the α1G subunit. The α1G KO mouse shows a complete loss of relay cell burst response (Kim et al., 2001), suggesting that this isoform of T-type calcium channel is essential for the bursting activity of the thalamic relay neurons. Using a highly specific antibody against α1G, our study has revealed the quantitative distribution of the α1G subunit in various parts of the dendritic arbor in the mouse dLGN neurons. The results suggest that α1G molecules are distributed with a uniform density over the somatodendritic plasma membrane compartments of the mouse dLGN cells.

### Regional distribution of α1G in the thalamus

In this study, we found immunoreactivity for the α1G subunit in the majority of the thalamic nuclei but not in the reticular thalamic nucleus in mice. The regional distribution of α1G immunoreactivity in the thalamus is in agreement with previously reported in situ hybridization studies (Zhang et al., 2002; the Allen Brain Atlas, Lein et al., 2007; Ernst et al., 2009) and an electrophysiological study (Chemin et al., 2002) which suggested the predominant expression of α1G in relay cells. However, our study differs from that of McKay et al. (2006) and Kovács et al. (2009), in which strong immunostaining in the TRN of rats and cats, respectively, was observed. In these studies, no tests in KO mice for the specificity of their antibodies were performed. While the difference in the species used might have been a cause for such a discrepancy in the immunoreactivity observed in the TRN, our data can be easily reconciled with the previous in situ hybridization study, which had no detectable expression of α1G in the rat TRN (Talley et al., 1999). It would be of future interest to examine the possible interspecies differences regarding the α1G localization in the TRN.

The presence of low-threshold calcium currents (LTCC) with fast kinetics in the rat TRN cells has been reported (Joksovic et al., 2005). In the study, the definitive subunit responsible for the LTCC was not identified due to the fact that both α1G and α1H subunits of the T-type calcium channel exhibit fast kinetics (Klöckner et al., 1999) and specific blockers against the individual subunits of the channels are not fully established.

Taken together, our data suggest that α1G is expressed in the majority of thalamic nuclei including

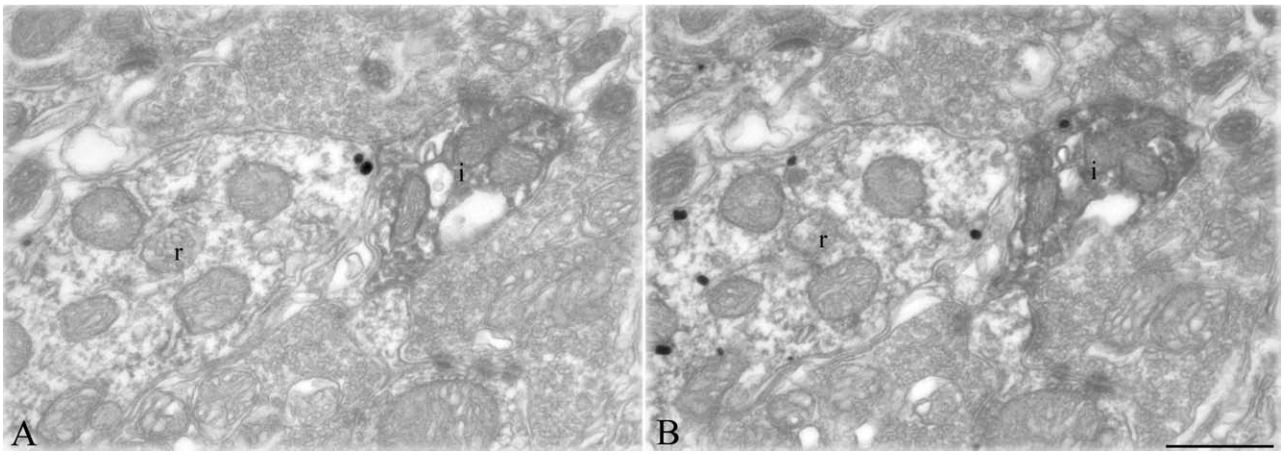


Figure 7. GABAergic interneurons showed weaker immunoreactivity for α1G than putative relay cells in the dLGN. The expression of α1G in GABAergic interneurons was investigated by double immunoelectron microscopy for α1G and GAD. GAD immunoreactivity was visualized by a peroxidase reaction and that for α1G was visualized by immunogold particles. Consecutive images (A and B) show a relay cell dendrite (r) and an interneuron dendrite (i) located adjacent to each other. Scale bar = 500 nm.

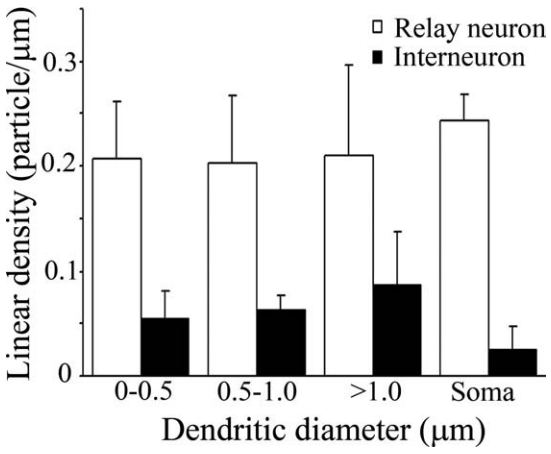


Figure 8. α1G expression level in interneurons was lower than that in relay cells in the dLGN. Bar graphs showing the average densities of the plasma membrane-bound immunogold particles for α1G in the dendrites, classified into three groups according to their diameter (<0.5 μm, 0.5–1 μm, >1 μm), and somata of the relay cells (open bar; n = 22 and 3 for dendrite and soma, respectively) and GABAergic interneurons (closed bar; n = 19 and 3 for dendrite and soma, respectively). The labeling densities in the interneurons were similar over different dendritic compartments (ANOVA, $P = 0.775$) and significantly lower than those in the relay cell ($P < 0.001$, Mann–Whitney *U*-test). In corroboration with the observation made from the single labeling experiment, no somatodendritic gradient of α1G immunogold particle was observed in the plasma membrane of the relay cells. Note that the relatively large magnitude of error bars (SEM) associated with each of the compartments suggests a considerable variability of the immunogold labeling density among the profiles with similar dendritic diameters.

dLGN but not in the TRN and that α1H rather than α1G may be the key component of LTCC showing fast kinetics in the TRN, at least in mice.

## Uniform distribution of α1G over somatodendritic plasma membrane of dLGN neurons and possible functional significance

The dendrites of principal relay neurons receive the glutamatergic afferents in a compartmentalized manner, with the sensory input generally contacting the proximal part of the relay cell dendrite and the cortical input preferentially contacting the distal part (Murphy and Sillito, 1987; Robson, 1993; Sherman and Guillery, 1998). Thalamic reticular axons make contacts throughout the dendritic arbor (Liu et al., 1995). In line with these morphological observations, the uniform distribution of α1G throughout the dendritic plasma membrane might suggest an efficient means of achieving rebound bursting during slow-wave sleep. That is, the GABA release from TRN axons can effectively de-inactivate dendritically localized T-type calcium channels and enables their activation with incoming glutamatergic signals (Contreras et al., 1993; Zhan et al., 2000). Thus, the expression of α1G in both the proximal and distal dendritic locations would imply the involvement of this subunit in the amplification of both the sensory input and the cortical input, thereby promoting the oscillatory activity of the relay cells.

Our study revealed that the density of the plasma membrane particles is uniform throughout the somatodendritic compartments of the dLGN relay neuron (Figs. 6A, 8). However, the ratios of surface area against volume change along the somatodendritic compartments; the soma has the smallest and the distal dendrite has the largest ratio. Taking this into consideration, the different ratios are likely to result in a proportionally larger effect of T-type calcium channels in the distal dendrite compared to the proximal dendrite. It has been suggested that the EPSP generated in the distal part will be attenuated on the way to the soma

(Bloomfield et al., 1987). Therefore, placing a larger number of calcium channels in the distal dendrite might be one of the ways to counteract the cable filtering effect.

Another line of evidence suggesting a higher density of T-type calcium channels in the proximal dendrites and soma stems from the dendritic cell attached patch recording (Williams and Stuart, 2000). Due to the technical difficulty in patching from very fine distal dendrites, these authors limited their study to within the proximal 60 μm length of the dendritic arbor. In view of the fact that the thalamic dendrites can extend as far as roughly 200 μm (Ohara and Havton, 1994), this study in effect investigated the channel distribution within a short dendritic segment.

Destexhe et al. (1998) performed an electrophysiological study of the T-type calcium channel density in the dendrites and soma of the ventrobasal neuron, another major thalamic relay neuron. The authors inferred a higher density of T-current in the distal dendrites than in the soma. They recorded the T-type current from dissociated cells, which lack most of the dendritic processes, and intact cells in slices and revealed T-type-mediated conductances of 8–14 pS/$\mu m^2$ in the dendrites and 4.5–7.6 times smaller values in the soma. By using computational studies, they suggested that T-type calcium channel density must be 5 times higher in the distal dendrite than in the soma to reproduce the current traces obtained from the intact thalamocortical cells recorded in slices. Assuming the single channel conductance of T-type channel as 7.5 pS (Perez-Reyes et al., 1998), the recorded conductance densities would be equivalent to 1.07–1.87 channels/$\mu m^2$ in the dendrites and 4.5–7.6 times smaller in the soma. Surprisingly, our preembedding immunogold labeling revealed an average labeling density of 2.60 particles/$\mu m^2$ for α1G in the relay cell dendrites. It is obvious that the channel density suggested by our immunogold labeling study is very likely to be underrepresented because the sensitivity of the method is unlikely to be 100%. However, the density value obtained here was even higher than that estimated in the recording experiment by Destexhe et al. Therefore, it is possible that this electrophysiological study is underestimating the actual numbers of T-channels in situ. This underestimation may compromise the computational conclusion leading to the higher density of T-channels in the distal dendrites.

Even though some studies have argued for a nonuniform distribution of T-channels, a recent computational study by Zomorrodi et al. (2008) suggested that the thalamic oscillations can be generated under uniform somatodendritic distribution of T-channels. Our experimental data together with their computational study raise the possibility that the nonuniform distribution of the T-type calcium channel is not a prerequisite for thalamic bursting.

In contrast to the uniform expression density of the plasma membrane α1G immunoparticles, the density of the intracellular membrane particles was highest in the soma and the proximal part of the dendrite and gradually decreased distally (Fig. 6B). The large amount of intracellular labeling observed in our experiment probably represents the newly synthesized α1G translocating from the site of synthesis to the plasma membrane. Some other cytoplasmic labeling may also represent the channels undergoing internalization and sequestration from the site of action.

Moreover, our quantitative analysis showed a large variability in the labeling density of the membrane-bound α1G even within the dendrites of similar diameters (Fig. 6A). This is consistent with the results of dendritic patch attached recordings in the dLGN, where the amplitude of the T-type calcium current was greatly variable in dendrites located at the same distance from the soma (Williams and Stuart, 2000). In the thalamic paraventricular nucleus, the calcium imaging experiments also revealed variability in the magnitude of the calcium transients among different dendrites (Richter et al., 2006).

## α1G expression in the dLGN interneurons

Due to the very small magnitude of rebound burst observed in interneurons, earlier studies suggested the lack of T-type calcium channels in these cells (McCormick and Pape, 1988). In later studies, it was shown that interneurons can generate burst firing in response to the injected current (Pape and McCormick, 1995; Munsch et al., 1997; Zhu et al., 1999; Broicher et al., 2007). The lack of burst firing in the interneurons in the earlier study was later reconciled to be due to the presence of A-type potassium current, which has an antagonistic effect in terms of net membrane current, thereby preventing the generation of low-threshold spikes (Pape et al., 1994). Here in our immunohistochemical study, we provide ultrastructural evidence for the presence of α1G in dLGN interneurons.

It is worth mentioning that some interneuron dendrites were not labeled throughout the serial section observed. The inclusion of these nonlabeled profiles resulted in the large error bars shown in Figure 8. It is conceivable that these immunonegative profiles express α1G at a low level; however, our method may have been insensitive to detect the minute amount of α1G. The fact that we did not observe immunolabeling in some of the interneurons might also suggest that there is a heterogeneous population of interneurons in the dLGN, and α1G may be expressed by an interneuronal subpopulation. There is indeed anatomical evidence indicating the presence of at least two populations of interneurons in the dLGN (Gabbott and Bacon, 1994).

## Technical considerations of our study

In contrast to our study that focused on 8-week-old adult mice, the electrophysiological studies were performed in young animals (postnatal days [P]12–16),

where the visual system is not fully mature and is still in the developmental stage. In view of the fact that the somatodendritic T-type calcium transients may vary during development (Pirchio et al., 1990; Yunker et al., 2003), the subcellular redistribution of α1G in adult mice compared to the postnatal age mice cannot be excluded. Comparing the present results with electrophysiological data obtained from the age-matched tissues would be informative and helpful in understanding the mechanisms underlying bursting activity in the dLGN neurons.

In our study, we could only assess the relative distance of individual dendritic profiles from the soma by measuring the dendritic cross-sectional diameter, and this method is less accurate than the direct measurement of the distances under a light microscope. Moreover, our analysis was performed by sampling profiles randomly from multiple cells in the area investigated, and a small-scale gradient, if any, of the channel localization might have been masked by variability of α1G expression levels among dLGN neurons.

It is also plausible that the quantification of the channel proteins detected by the immunogold method may not necessarily correlate with the expression density of the functional channel. It has been suggested that calcium channels may either be in a phosphorylated or nonphosphorylated state (for review, see Catterall, 2000) and the phosphorylation of α1G molecules potentiates T-type calcium current amplitude in the thalamocortical neurons (Leresche et al., 2004; Park et al., 2006). Thus, even if the channels are distributed uniformly in situ, the electrophysiological responsiveness of these channels might differ at various neuronal compartments depending on their phosphorylation states (Zomorrodi et al., 2008).

Our study did not reveal any obvious preference of α1G molecules for the synaptic sites. However, in the preembedding method most of the antibodies fail to detect target antigens located at the postsynaptic sites (for review, see Masugi-Tokita and Shigemoto, 2007). Therefore, our observation that immunogold particles for α1G were not present within the postsynaptic densities may need to be interpreted with caution.

In conclusion, the present results revealed that the α1G subunit of T-type calcium channels are uniformly distributed in the somatodendritic plasma membrane compartments of dLGN neurons. Further studies on the relative spatial localization of α1G to other ionic channels important for thalamic bursting might substantiate our current understanding of rhythmic activities of thalamic neurons.

## ACKNOWLEDGMENTS

We thank Drs. M. Kano and K. Sakimura for providing α1G-deficient mice. We thank Dr. K. Matsui for valuable discussions during the initial phase of article preparation.

## LITERATURE CITED

Anderson MP, Mochizuki T, Xie J, Fischler W, Manger JP, Talley EM, Scammell TE, Tonegawa S. 2005. Thalamic Cav3.1 T-type $Ca^{2+}$ channel plays a crucial role in stabilizing sleep. Proc Natl Acad Sci U S A 102:1743–1748.

Arcelli P, Frassoni C, Regondi MC, Biasi SD, Spreafico R. 1997. GABAergic Neurons in mammalian thalamus: a marker of thalamic complexity. Brain Res Bull 42:27–37.

Barthó P, Payne JA, Freund TF, Acsády L. 2004. Differential distribution of the KCl cotransporter KCC2 in thalamic relay and reticular nuclei. Eur J Neurosci 20:965–975.

Bloomfield SA, Hamos JE, Sherman SM. 1987. Passive cable properties and morphological correlates of neurones in the lateral geniculate nucleus of the cat. J Physiol (Lond) 383:653–692.

Broicher T, Kanyshkova T, Landgraf P, Rankovic V, Meuth P, Meuth SG, Pape HC, Budde T. 2007. Specific expression of low-voltage-activated calcium channel isoforms and splice variants in thalamic local circuit interneurons. Mol Cell Neurosci 36:132–145.

Catterall WA. 2000. Structure and regulation of voltage-gated $Ca^{2+}$ channels. Annu Rev Cell Dev Biol 16:521–555.

Chang YC, Gottlieb DI. 1988. Characterization of the proteins purified with monoclonal antibodies to glutamic acid decarboxylase. J Neurosci 8:2123–2130.

Chemin J, Monteil A, Perez-Reyes E, Bourinet E, Nargeot J, Lory P. 2002. Specific contribution of human T-type calcium channel isotypes (α1G, α1H and α1I) to neuronal excitability. J Physiol 540:3–14.

Contreras D, Curro Dossi R, Steriade M. 1993. Electrophysiological properties of cat reticular thalamic neurones in vivo. J Physiol (Lond) 470:273–294.

Destexhe A, Neubig M, Ulrich D, Huguenard J. 1998. Dendritic low-threshold calcium currents in thalamic relay cells. J Neurosci 18:3574–3588.

Ernst WL, Zhang Y, Yoo JW, Ernst SJ, Noebels JL. 2009. Genetic enhancement of thalamocortical network activity by elevating α1G mediated low-voltage-activated calcium current induces pure absence epilepsy. J Neurosci 29:1615–1625.

Fiala JC. 2005. Reconstruct: a free editor for serial section microscopy. J Microsc 218:52–61.

Gabbott PLA, Bacon SJ. 1994. Two type of interneurons in the dorsal lateral geniculate nucleus of the rat: a combined NADPH diaphorase histochemical and GABA-immunocytochemical study. J Comp Neurol 350:281–301.

Hanson JE, Smith Y. 2002. Subcellular distribution of high-voltage-activated calcium channel subtypes in rat globus pallidus neurons. J Comp Neurol 442:89–98.

Hildebrand ME, Isope P, Miyazaki T, Nakaya T, Garcia E, Feltz A, Schneider T, Hescheler J, Kano M, Sakimura K, Watanabe M, Dieudonne S, Snutch TP. 2009. Functional coupling between mGluR1 and Cav3.1 T-type calcium channels contributes to parallel fibre-induced fast calcium signaling within purkinje cell dendritic spines. J Neurosci 31:9668–9682.

Huguenard JR. 1996. Low-threshold calcium currents in central nervous system neurons. Annu Rev Physiol 58:329–348.

Jahnsen H, Llinás R. 1984. Electrophysiological properties of guinea-pig thalamic neurones: an in vitro study. J Physiol 349:205–226.

Joksovic PM, Bayliss DA, Todorovic SM. 2005. Different kinetic properties of two T-type $Ca^{2+}$ currents of rat reticular thalamic neurones and their modulation by enflurane. J Physiol 566:125–142.

Jones SW. 1998. Overview of voltage dependent calcium channels. J Bioenerg Biomemb 30:299–312.

Jones EG. 2007. The thalamus, 2nd ed. New York: Cambridge University Press.

Kim D, Song I, Keum S, Lee T, Jeong MJ, Kim SS, McEnery MW, Shin HS. 2001. Lack of burst firing of thalamocortical

relay neurons and resistance to absence seizures in mice lacking α1G T-type calcium channels. Neuron 31:35–45.
Klöckner U, Lee JH, Cribbs LL, Daud A, Hescheler J, Pereverzev A, Perez-Reyes E, and Schneider T. 1999. Comparison of the $Ca^{2+}$ currents induced by expression of three cloned α1 subunits, α1G, α1H and α 1I, of low-voltage-activated T-type $Ca^{2+}$ channels. Eur J Neurosci 11:4171–4178.
Kovács K, Sík A, Ricketts C, Timofeev I. 2009. Subcellular distribution of low-voltage activated T-type $Ca^{2+}$ channel subunits (Cav3.1 and Cav3.3) in reticular thalamic neurons of the cat. J Neurosci Res 88:448–460.
Kulik A, Nakadate K, Hagiwara A, Fukazawa Y, Lujan R, Saito H, Suzuki N, Futatsugi A, Mikoshiba K, Frotscher M, Shigemoto R. 2004. Immunocytochemical localization of the α1A subunit of the P/Q-type calcium channel in the rat cerebellum. Eur J Neurosci 19:2169–2178.
Lee J, Kim D, Shin HS. 2004. Lack of delta waves and sleep disturbances during non-rapid eye movement sleep in mice lacking α1G-subunit of T-type calcium channels. Proc Natl Acad Sci U S A 101:18195–18199.
Lein ES, Hawrylycz MJ, Ao N, et al. 2007. Genome-wide atlas of gene expression in the adult mouse brain. Nature 445: 168–176.
Leresche N, Hering J. Lambert RC. 2004. Paradoxical potentiation of neuronal T-type $Ca^{2+}$ current by ATP at resting membrane potential. J Neurosci 24:5592–5602.
Lieberman AR, Webster KE. 1974. Aspects of the synaptic organization of intrinsic neurons in the dorsal lateral geniculate nucleus. An ultrastructural study of the normal and of the experimentally deafferented nucleus in the rat. J Neurocytol 3:677–710.
Liu XB, Honda CN, Jones EG. 1995. Distribution of four types of synapse on physiologically identified relay neurons in the ventral posterior thalamic nucleus of the cat. J Comp Neurol 352:69–91.
Masugi-Tokita M, Shigemoto R. 2007. High-resolution quantitative visualization of glutamate and GABA receptors at central synapses. Curr Opin Neurobiol 17:387–393.
McCormick DA, Pape HC. 1988. Acetylcholine inhibits identified interneurons in the cat lateral geniculate nucleus. Nature 334:246–248.
McKay BE, McRory JE, Molineux ML, Hamid J, Snutch TP, Zamponi GW, Turner RW. 2006. Ca(V)3 T-type calcium channel isoforms differentially distribute to somatic and dendritic compartments in rat central neurons. Eur J Neurosci. 24: 2581–2594.
Munsch T, Budde T, Pape HC. 1997. Voltage activated intracellular calcium transients in thalamic relay cells and interneurons. Neuroreport 8:2411–2418.
Murphy PC, Sillito AM. 1987. Corticofugal feedback influences the generation of length turning in the visual pathway. Nature 329:727–729.
Ohara PT, Havton LA. 1994. Dendritic architecture of rat somatosensory thalamocortical projection neurons. J Comp Neurol 341:159–171.
Ohara PT, Lieberman AR, Hunt SP, Wu JY. 1983. Neural elements containing glutamic acid decarboxylase in the dorsal lateral geniculate nucleus of the rat; immunohistochemical studies by light and electron microcopy. Neuroscience 8: 189–211.
Pape HC, McCormick DA. 1995. Electrophysiological and pharmacological properties of interneurons in the cat dorsal lateral geniculate nucleus. Neuroscience 68:1105–1125.
Pape HC, Budde T, Mager R, Kisvarday ZF. 1994. Prevention of $Ca^{2+}$-mediated action potentials in GABAergic local circuit neurones of rat thalamus by a transient $K^{+}$ current. J Physiol (Lond) 478:403–422.
Park JY, Kang HW, Moon HJ, Huh SU, Jeong SW, Soldatov NM, Lee JH. 2006. Activation of protein kinase C augments T-type $Ca^{2+}$ channel activity without changing channel surface density. J Physiol (Lond) 577:513–523.
Paxinos G. 1995. The rat nervous system, 2nd ed. Sydney: Academic Press.
Perez-Reyes E. 2003. Molecular physiology of low-voltage-activated T-type calcium channels. Physiol Rev 83:117–161.
Perez-Reyes E, Cribbs LL, Daud A, Lacerda AE, Barclay J, Williamson MP, Fox M, Rees M, Lee J-H. 1998. Molecular characterization of a neuronal low-voltage-activated T-type calcium channel. Nature 391:896–900.
Pirchio M, Lightowler S, Crunelli V. 1990. Postnatal development of the T calcium current in cat thalamocortical cells. Neuroscience 38:39–45.
Rhodes PA, Llinas R. 2005. A model of thalamocortical relay cells. J Physiol (Lond) 565:765–781.
Richter TA, Kolaj M, Renaud LP. 2006. Heterogeneity in low voltage-activated $Ca^{2+}$ channel-evoked $Ca^{2+}$ responses within neurons of the thalamic paraventricular nucleus. Eur J Neurosci 24:1316–1324.
Robson JA. 1993. Qualitative and quantitative analysis of the patterns of retinal input to neurons in the dorsal lateral geniculate nucleus of the cat. J Comp Neurol 334:324–336.
Sherman SM, Guillery RW. 1998. On the actions that one nerve cell can have on another: distinguishing "drivers" from "modulators." Proc Natl Acad Sci U S A 95:7121–7126.
Song I, Kim D, Choi S, Sun M, Kim Y, Shin HS. 2004. Role of the α1G T-type calcium channel in spontaneous absence seizures in mutant mice. J Neurosci 24:5249–5257.
Steriade M, Llinas RR. 1988. The functional state of the thalamus and the associated neuronal interplay. Physiol Rev 68:649–742.
Talley EM, Cribbs LL, Lee J, Daud A, Perez-Reyes E, Bayliss DA. 1999. Differential distribution of three members of a gene family encoding low voltage-activated (T-type) calcium channels. J Neurosci 19:1895–1911.
Williams SR, Stuart GJ. 2000. Action potential backpropagation and somato-dendritic distribution of ion channels in thalamocortical neurons. J Neurosci 20:1307–1317.
Yunker AMR, Sharp AH, Sundarrad S, Ranganathan V, Copeland TD, McEnery MW. 2003. Immunological characterization of T-type voltage dependent calcium channel Cav3.1 (alpha1G) and Cav3.3 (alpha1I) isoforms reveal differences in their localization, expression and neural development. Neuroscience 117:321–335.
Zhan XJ, Cox CL, Sherman SM. 2000. Dendritic depolarization efficiently attenuates Low-threshold calcium spikes in thalamic relay cells. J Neurosci 20:3909–3914.
Zhang Y, Mori M, Burgess DL, Noebels JL. 2002. Mutations in high-voltage-activated calcium channel genes stimulate low-voltage-activated currents in mouse thalamic relay neurons. J Neurosci 22:6362–6371.
Zhou Q, Godwin DW, O'Malley DM, Adams PR. 1997. Visualization of calcium influx through channels that shape the burst and tonic firing modes of thalamic relay cells. J Neurophysiol 77:2816–2825.
Zhu JJ, Lytton WW, Xue JT, Uhlrich DJ. 1999. An intrinsic oscillation in interneurons of the rat lateral geniculate nucleus. J Neurophysiol 81:702–711.
Zhuravleva SO, Kostyuk PG, Shuba YM. 2001. Subtypes of low voltage-activated $Ca^{2+}$ channels in laterodorsal thalamic neurons: possible localization and physiological roles. Eur J Physiol 441:832–839.
Zomorrodi R, Kröger H, Timofeev I. 2008. Modeling thalamocortical cell: impact of $Ca^{2+}$ channel distribution and cell geometry on firing pattern. Front Comput Neurosci 2:5.